SUPPLEMENTAL INFORMATION

Protonation drives the conformational switch in the multidrug transporter LmrP.

Matthieu Masureel[1,3], Chloé Martens[1,3], Richard A Stein[2], Smriti Mishra[2], Jean-Marie Ruysschaert[1], Hassane S Mchaourab[2,4] and Cédric Govaerts[1,4].

[1]Laboratory for the Structure and Function of Biological Membranes, Center for Structural Biology and Bioinformatics, Université Libre de Bruxelles, CP 206/2, Bd du Triomphe, 1050 Brussels, Belgium

[2]Department of Molecular Physiology and Biophysics, Vanderbilt University Medical Center, 2215 Garland Avenue, Nashville, TN 37232, USA

[3]These authors contributed equally to this work.

[4]These authors are co-last authors.

Correspondence should be addressed to H.M. (hassane.mchaourab@vanderbilt.edu) and C.G. (cgovaert@ulb.ac.be)

Supplementary Figures

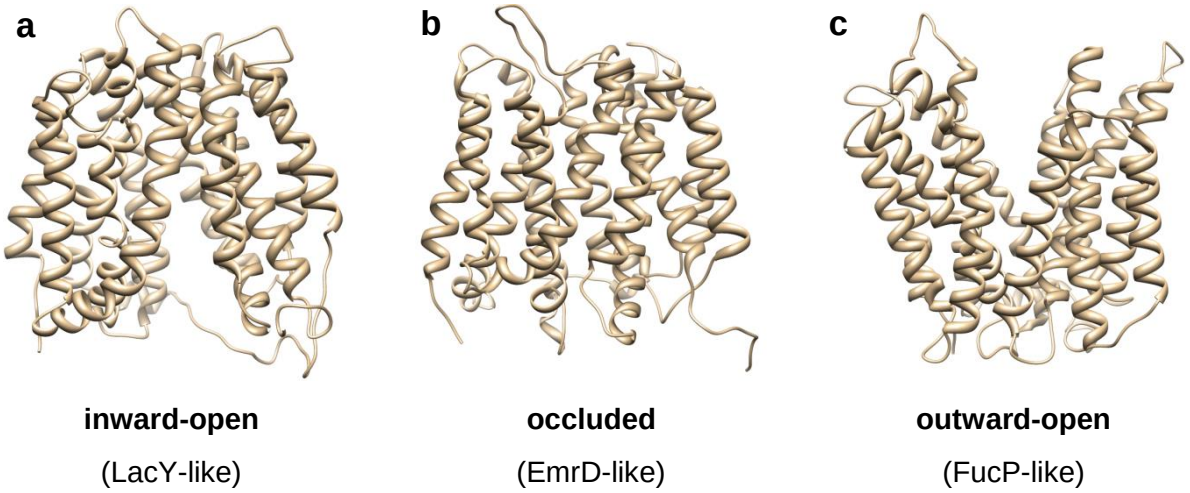

Supplementary Figure 1 | Ribbon diagram of LmrP models that represent canonical states required for alternating access-type transport. The *E. coli* structures of sugar importer LacY[8], multidrug exporter EmrD[11] and fucose importer FucP[9] represent inward-open, occluded and outward-open conformations, respectively, with the extracellular side at the top. We generated these models by aligning the LmrP sequence onto the sequence of the structural templates (see METHODS for more details) and using Modeller[51]. The structures depicted were generated using Chimera[52].

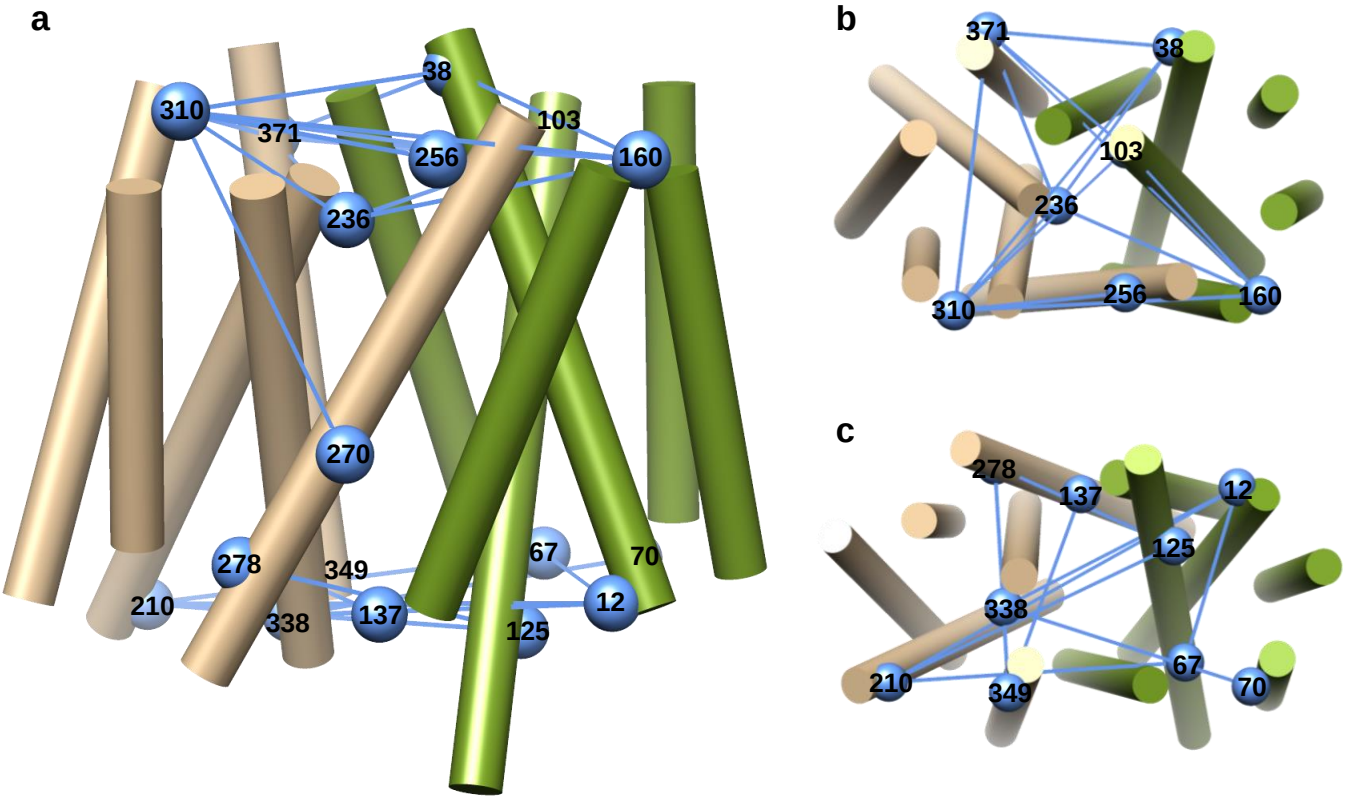

Supplementary Figure 2 | Schematic representation of LmrP modeled on the EmrD structure. TM segments are depicted as cylinders. The N-terminal half of the protein (TMs 1-6) is colored green, the C-terminal half (TMs 7-12) colored brown. Positions of engineered cysteines (blue spheres) and the pairwise distance measurements are shown: (**a**) viewed from the side of the membrane (extracellular side on top), (**b**) viewed atop from the extracellular side, (**c**) viewed atop from the intracellular side.

Supplementary Figures

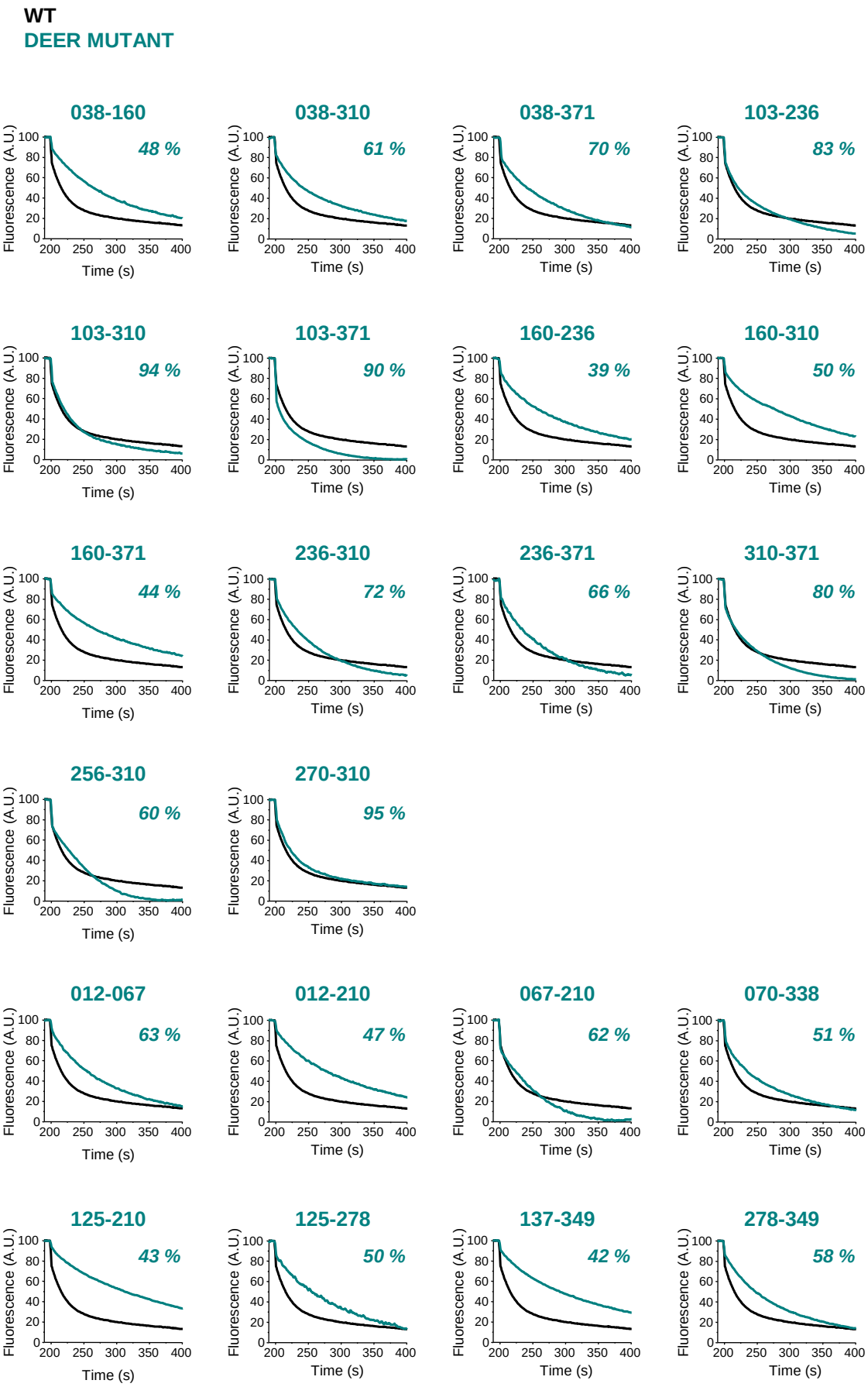

Supplementary Figure 3 | Transport activity assay of double cysteine mutants. LmrP-dependent Hoechst 33342 extrusion is monitored in inside-out membrane vesicles by a fluorescence-based assay (see METHODS). Values were normalized for fluorescence intensity and total protein amount. Addition of ATP activates the endogenous F_0/F_1 – ATPase leading to formation of a transmembrane proton gradient, thus triggering LmrP activity. The initial transport rates were calculated using the first 15 seconds and normalized relative to wild-type LmrP (100 %).

Supplementary Figures

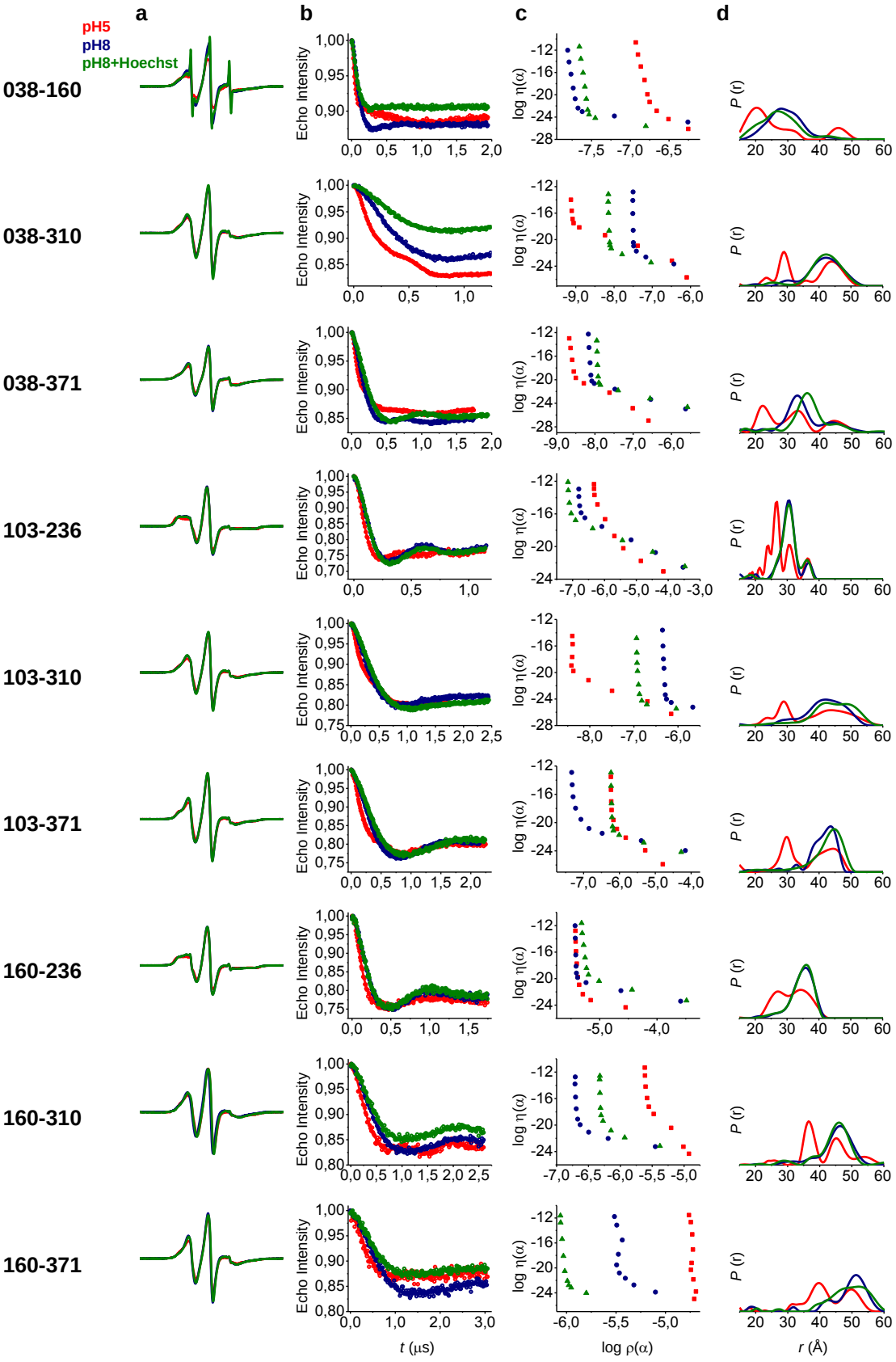

Supplementary Figure 4 | CW-EPR and DEER data analysis for spin label pairs on the extracellular side of LmrP. (**a**) Superposition of the EPR lineshapes of spin labeled pairs in DDM micelles at pH 5 (red), pH 8 (blue) and pH 8+Hoechst 33342 (green) demonstrated little change in spin label dynamics indicating that the local environment of the spin labels does not change substantially. (**b**) Time-dependent decay of the DEER signal (circles) and the fits (line) determined from Tikhonov regularization. (**c**) The optimum regularization parameter was chosen from the elbow of the L-curves to obtain the distance distributions shown in **Figures 1** and **4** and panel **d**. (**d**) DEER distance distributions.

Supplementary Figures

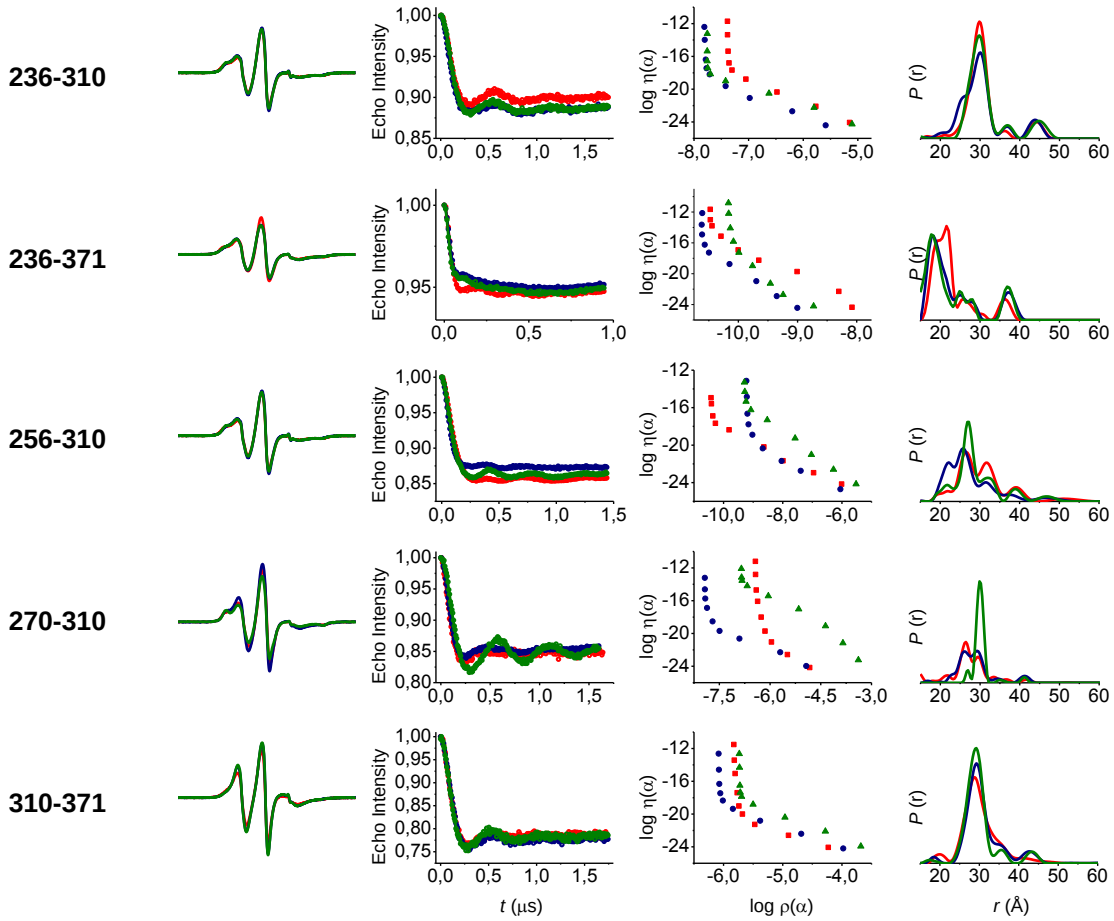

Supplementary Figure 4 (continued) | CW-EPR and DEER data analysis for spin label pairs on the extracellular side of LmrP. (**a**) Superposition of the EPR lineshapes of spin labeled pairs in DDM micelles at pH 5 (red), pH 8 (blue) and pH 8+Hoechst 33342 (green) demonstrated little change in spin label dynamics indicating that the local environment of the spin labels does not change substantially. (**b**) Time-dependent decay of the DEER signal (circles) and the fits (line) determined from Tikhonov regularization. (**c**) The optimum regularization parameter was chosen from the elbow of the L-curves to obtain the distance distributions shown in **Figures 1** and **4** and panel **d**. (**d**) DEER distance distributions.

Supplementary Figures

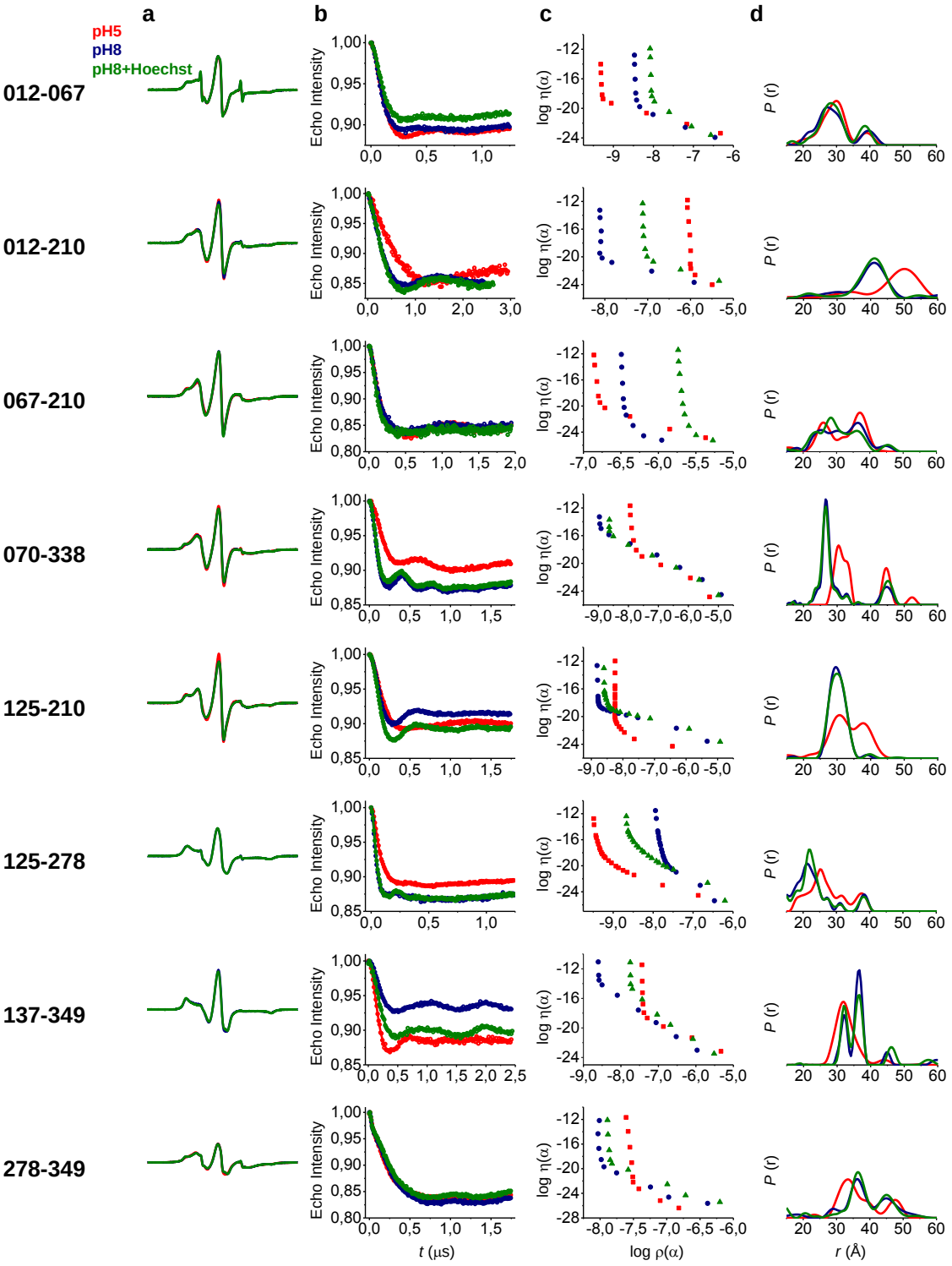

Supplementary Figure 5 | CW-EPR and DEER data analysis for spin label pairs on the intracellular side of LmrP. (**a**) Superposition of the EPR lineshapes of spin labeled pairs in DDM micelles at pH 5 (red), pH 8 (blue) and pH 8 + Hoechst 33342 (green) demonstrated little change in spin label dynamics for each intermediate state, indicating that the local environment of the spin labels does not change substantially. (**b**) Time-dependent decay of the DEER signal (circles) and the fit (line) determined from Tikhonov regularization. (**c**) The optimum regularization parameter was chosen from the elbow of the L-curves to obtain the distance distributions shown in **Figure 2** and panel **d**. (**d**) DEER distance distributions.

012–210 (TM1–TM7, intracellular)

pH 5

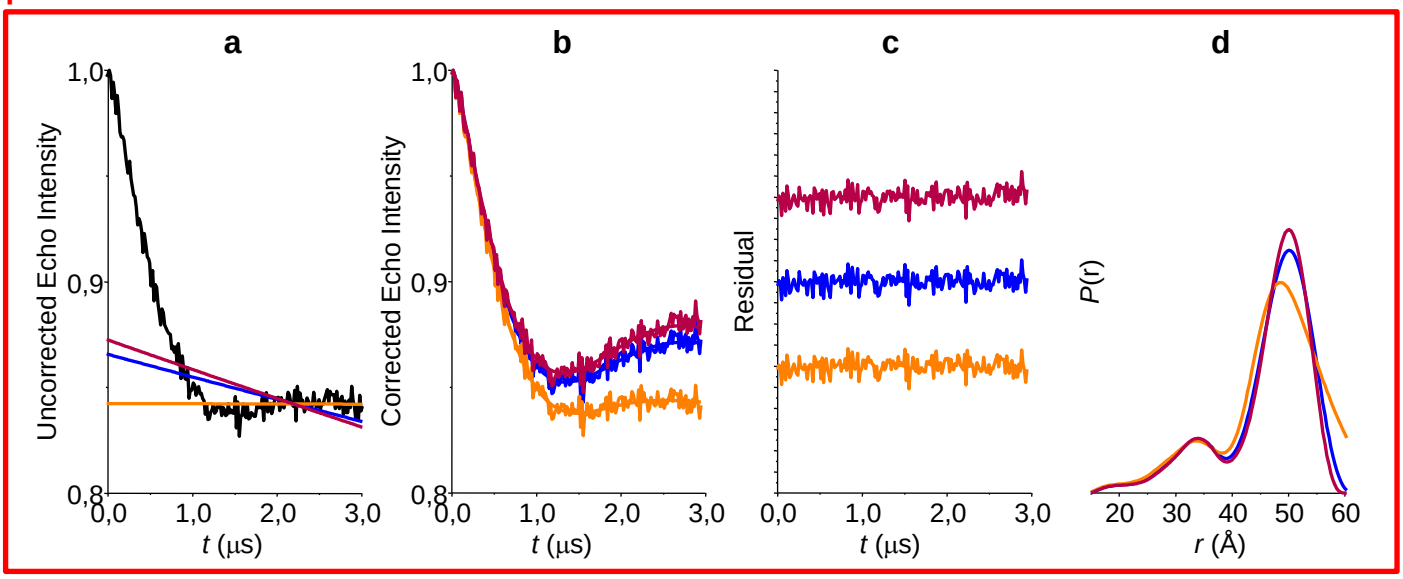

pH 8

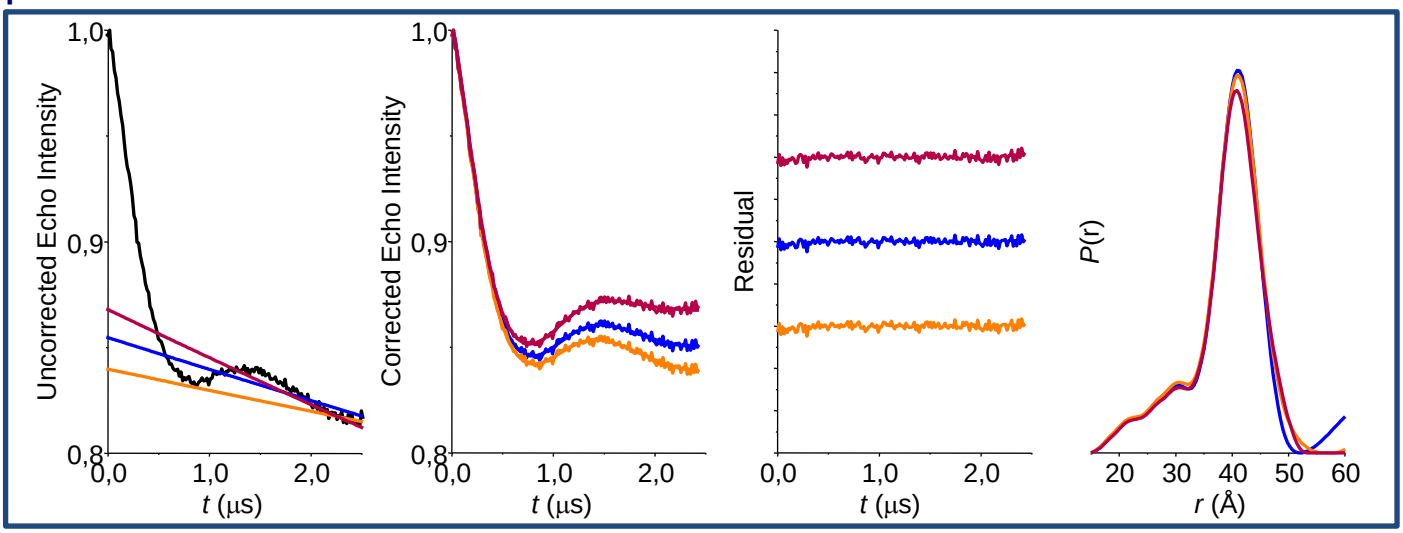

pH 8 + Hoechst

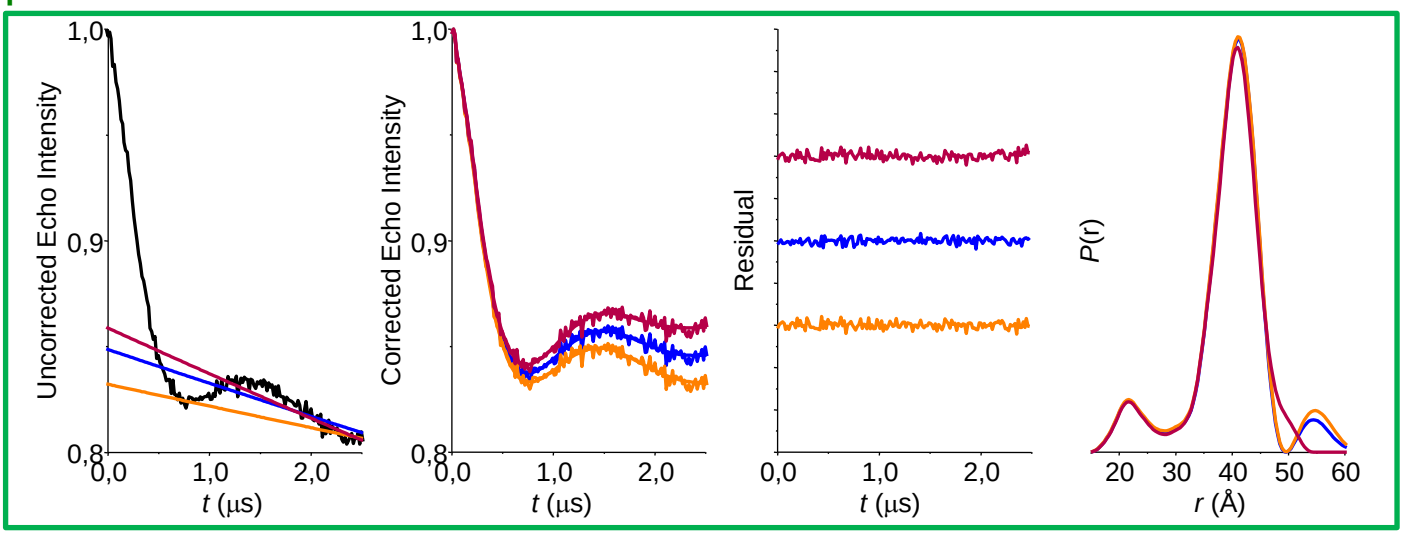

Supplementary Figure 6 | Variation in the background slope does not affect the overall profile of DEER distance distributions. Representative analysis of DEER data for cysteine pairs on the intracellular (012-210 & 125-210) and extracellular sides (38-310 & 160-236) under the conditions tested (pH 5, pH 8, pH 8 + Hoechst 33342). The background slope was increased or decreased (magenta and orange curves, respectively) relative to the optimum slope (blue curves) while maintaining the RMSD between DEER data and fits within 10 %. (**a**) Raw DEER decays (black curve) and (**b**) the background curves (colored curves) used to generate baselines corrected DEER decays. (**c**) Residuals between data and theoretical curves shown in the same color as the background curves. (**d**) Distance distributions resulting from the data fits shown in the same color as the background curves.

125–210 (TM4–TM7, intracellular)

pH 5

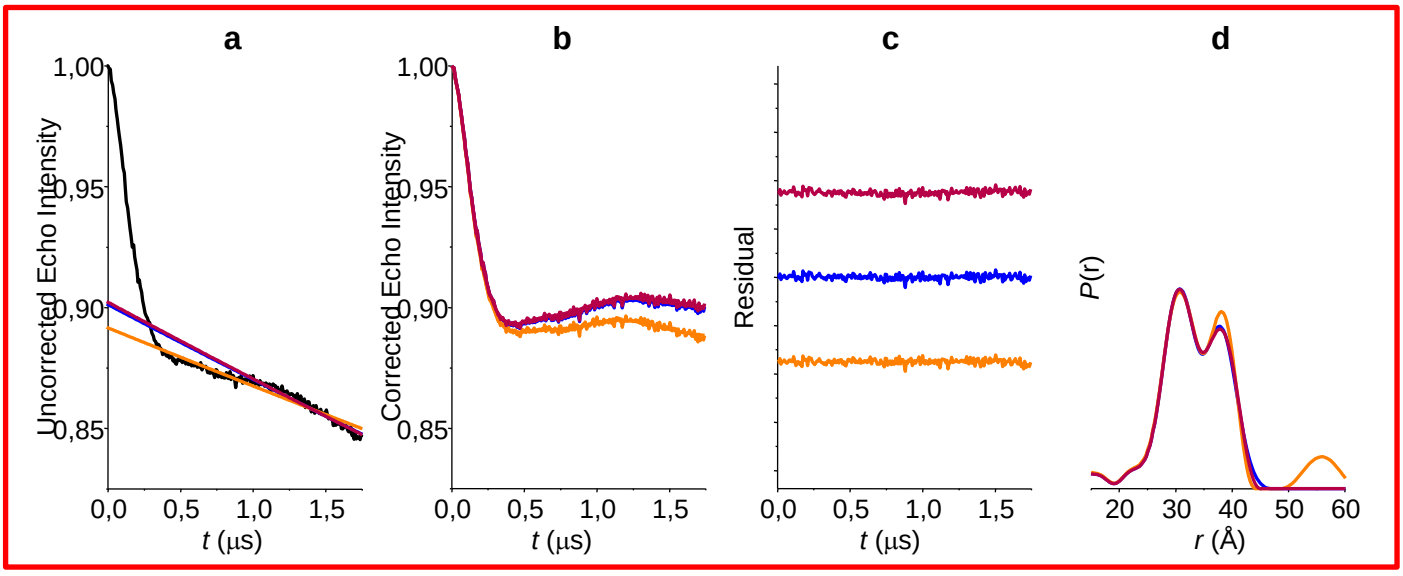

pH 8

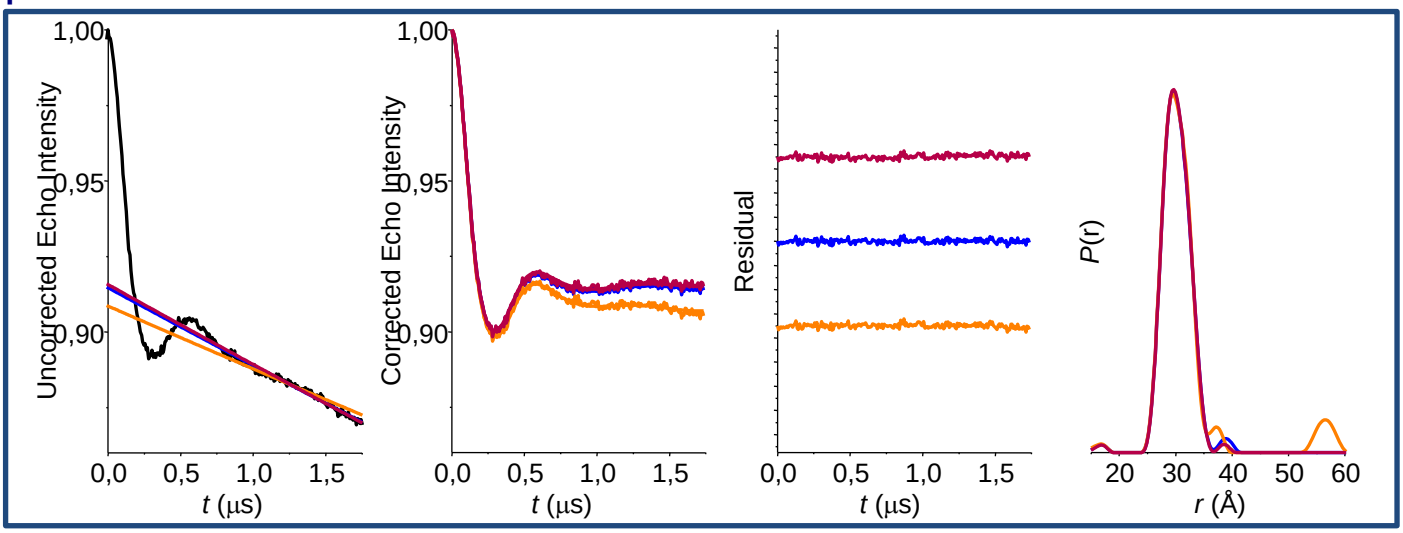

pH 8 + Hoechst

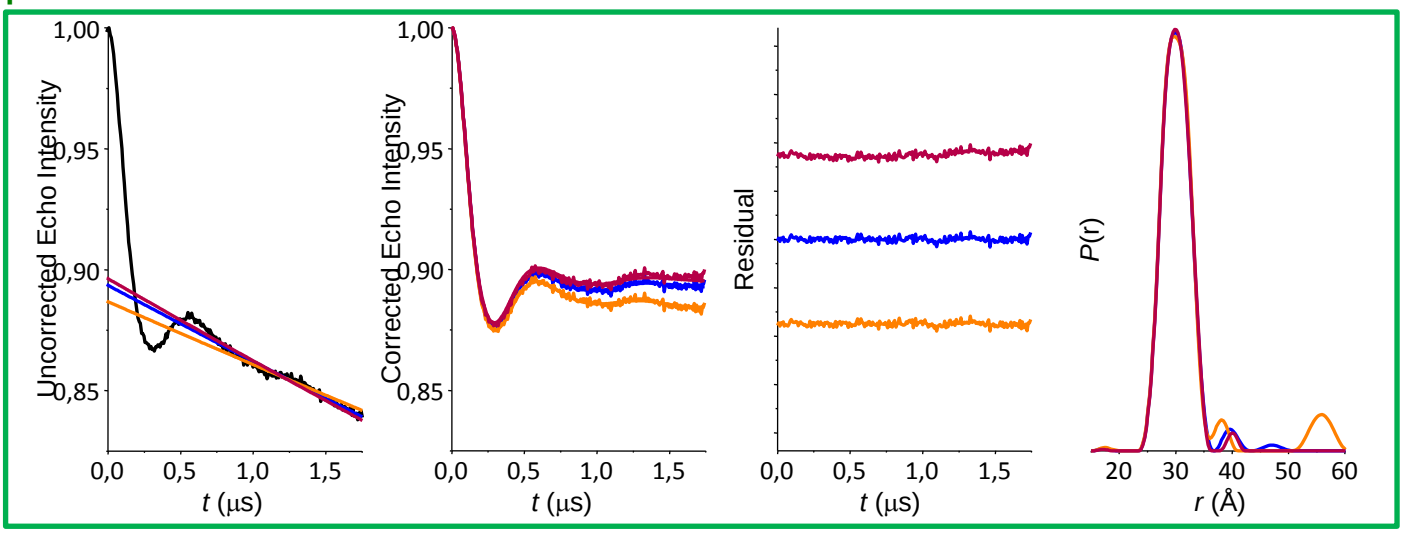

Supplementary Figure 6 (continued) | Variation in the background slope does not affect the overall profile of DEER distance distributions. Representative analysis of DEER data for cysteine pairs on the intracellular (012-210 & 125-210) and extracellular sides (38-310 & 160-236) under the conditions tested (pH 5, pH 8, pH 8 + Hoechst 33342). The background slope was increased or decreased (magenta and orange curves, respectively) relative to the optimum slope (blue curves) while maintaining the RMSD between DEER data and fits within 10 %. (**a**) Raw DEER decays (black curve) and (**b**) the background curves (colored curves) used to generate baselines corrected DEER decays. (**c**) Residuals between data and theoretical curves shown in the same color as the background curves. (**d**) Distance distributions resulting from the data fits shown in the same color as the background curves.

038–310 (TM1–TM10, extracellular)

pH 5

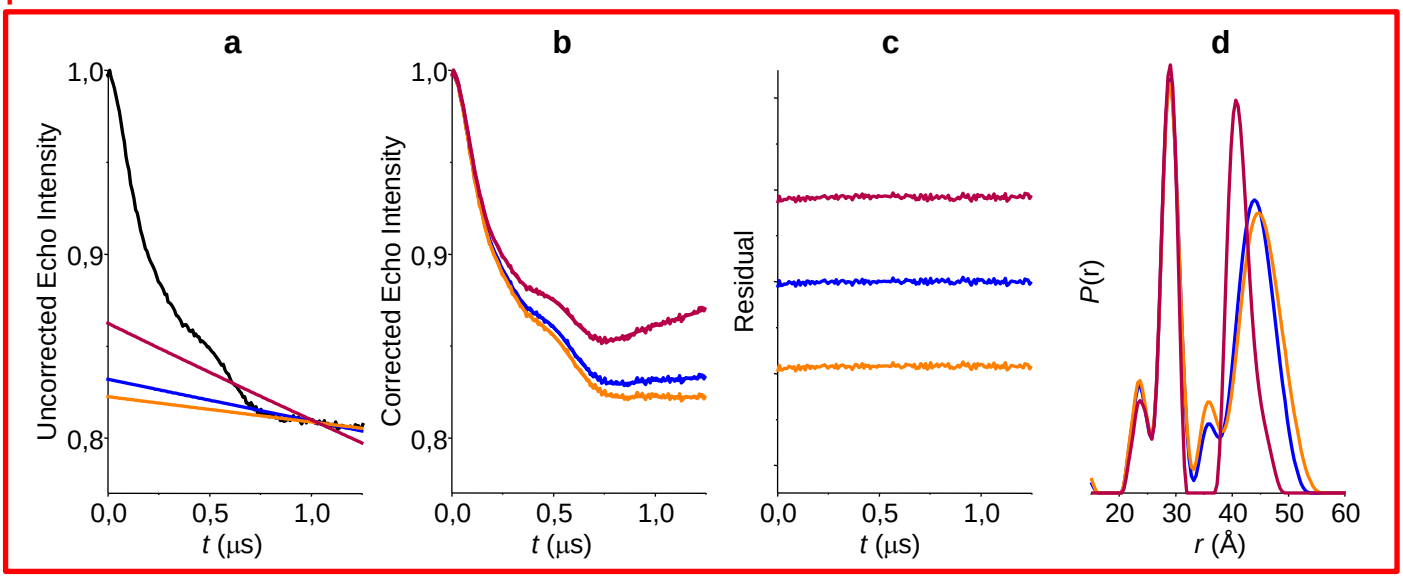

pH 8

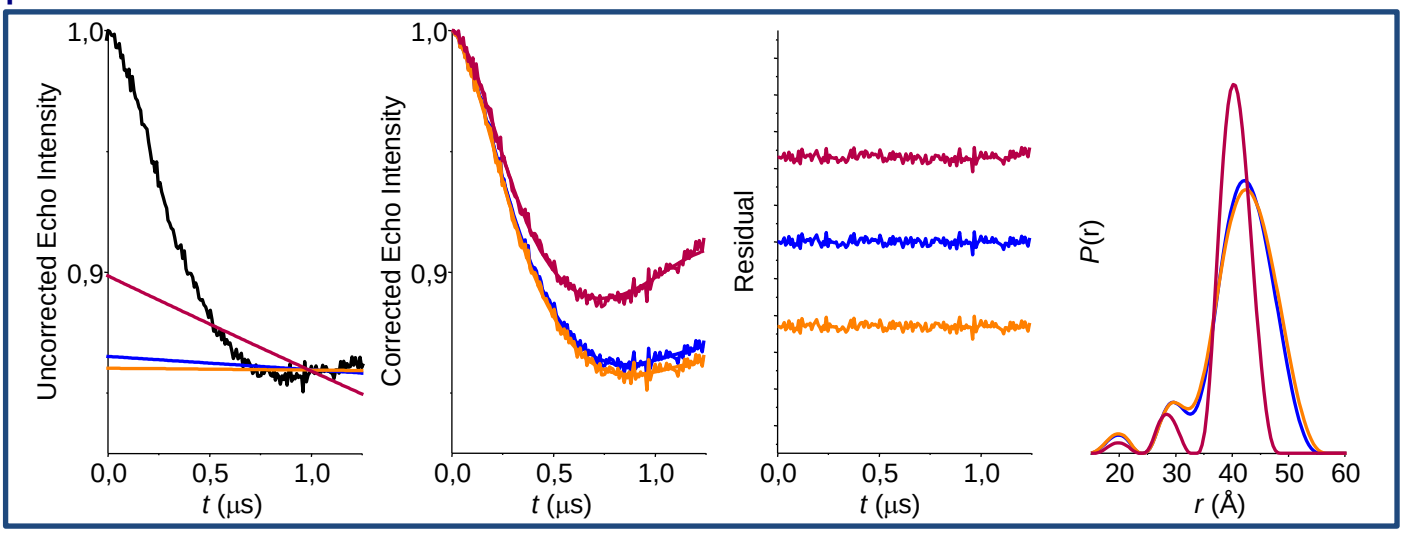

pH 8 + Hoechst

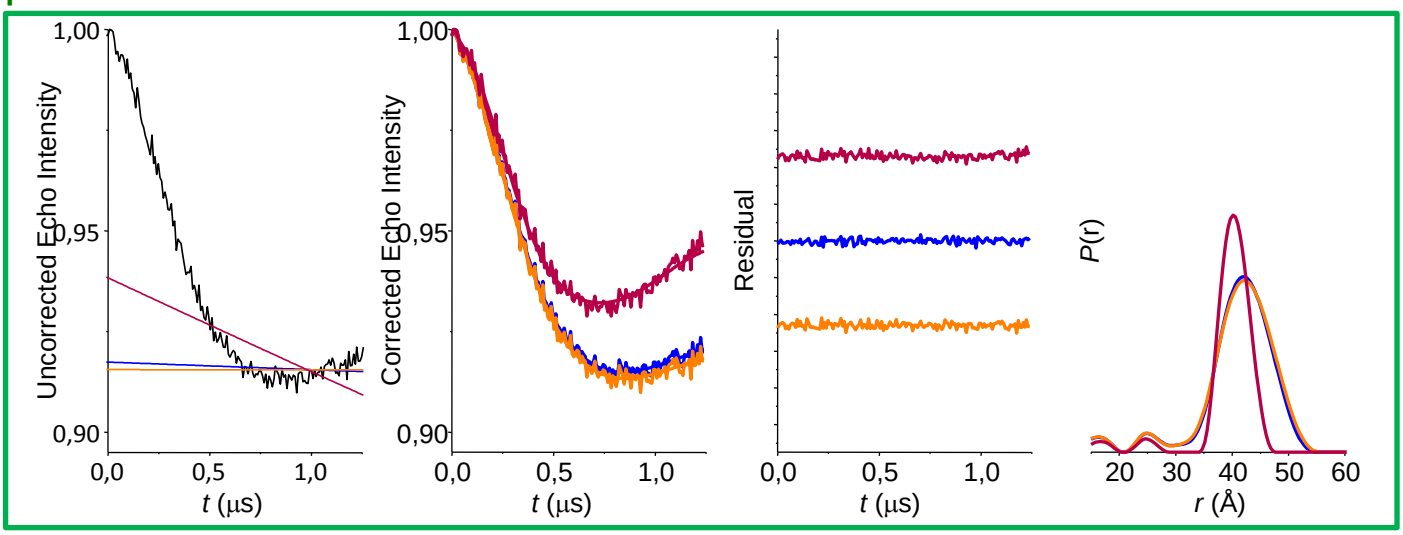

Supplementary Figure 6 (continued) | Variation in the background slope does not affect the overall profile of DEER distance distributions. Representative analysis of DEER data for cysteine pairs on the intracellular (012-210 & 125-210) and extracellular sides (38-310 & 160-236) under the conditions tested (pH 5, pH 8, pH 8 + Hoechst 33342). The background slope was increased or decreased (magenta and orange curves, respectively) relative to the optimum slope (blue curves) while maintaining the RMSD between DEER data and fits within 10 %. (**a**) Raw DEER decays (black curve) and (**b**) the background curves (colored curves) used to generate baselines corrected DEER decays. (**c**) Residuals between data and theoretical curves shown in the same color as the background curves. (**d**) Distance distributions resulting from the data fits shown in the same color as the background curves.

160–236 (TM5–TM7, extracellular)

pH 5

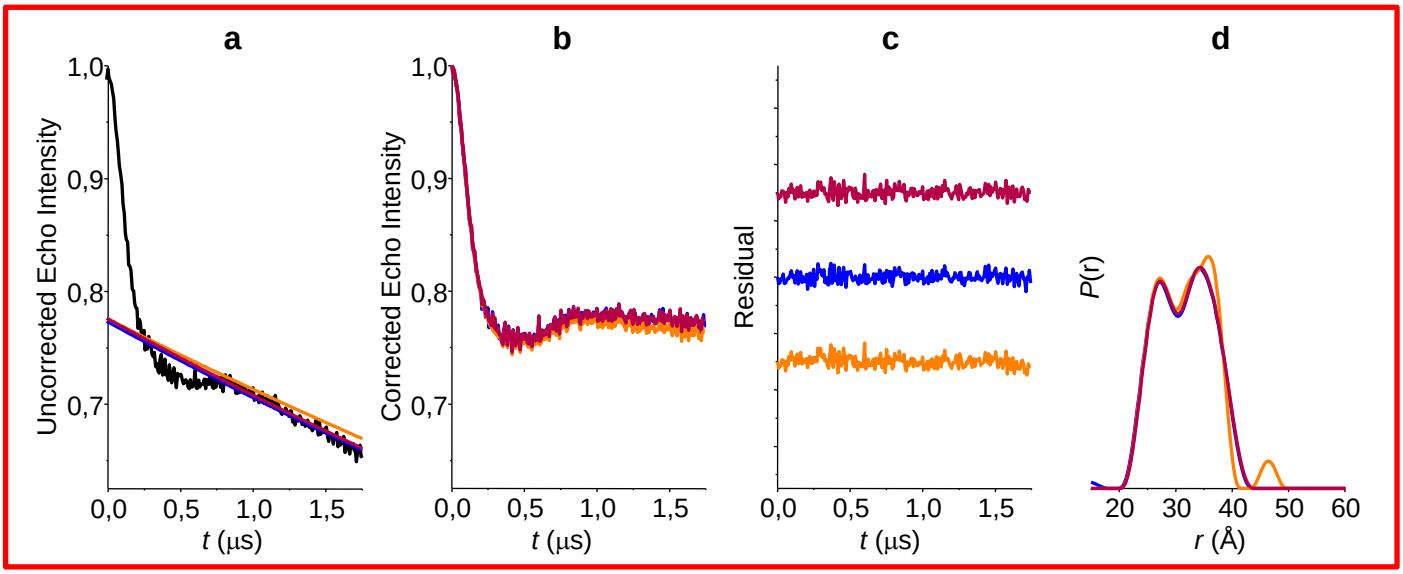

pH 8

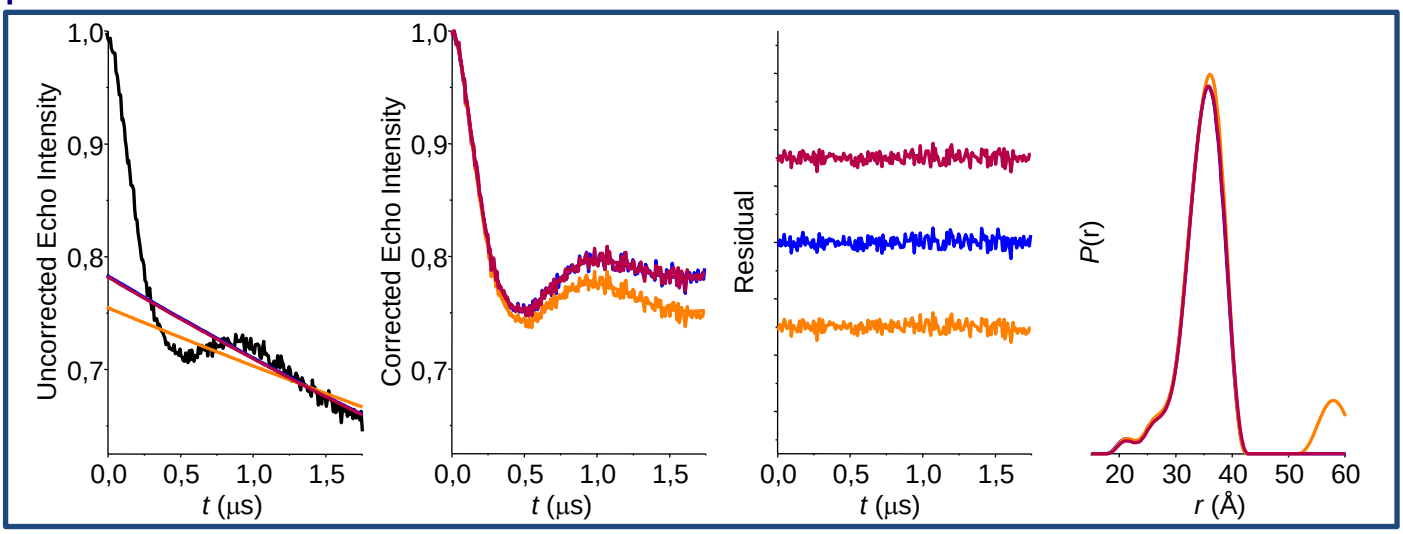

pH 8 + Hoechst

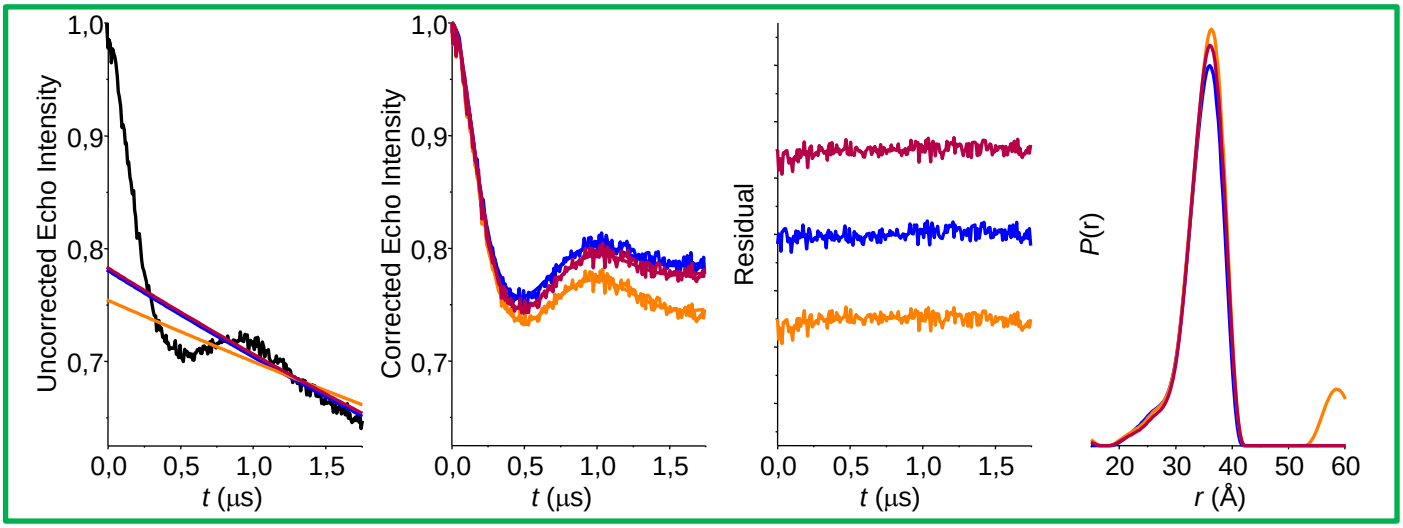

Supplementary Figure 6 (continued) | Variation in the background slope does not affect the overall profile of DEER distance distributions. Representative analysis of DEER data for cysteine pairs on the intracellular (012-210 & 125-210) and extracellular sides (38-310 & 160-236) under the conditions tested (pH 5, pH 8, pH 8 + Hoechst 33342). The background slope was increased or decreased (magenta and orange curves, respectively) relative to the optimum slope (blue curves) while maintaining the RMSD between DEER data and fits within 10 %. (**a**) Raw DEER decays (black curve) and (**b**) the background curves (colored curves) used to generate baselines corrected DEER decays. (**c**) Residuals between data and theoretical curves shown in the same color as the background curves. (**d**) Distance distributions resulting from the data fits shown in the same color as the background curves.

Supplementary Figures

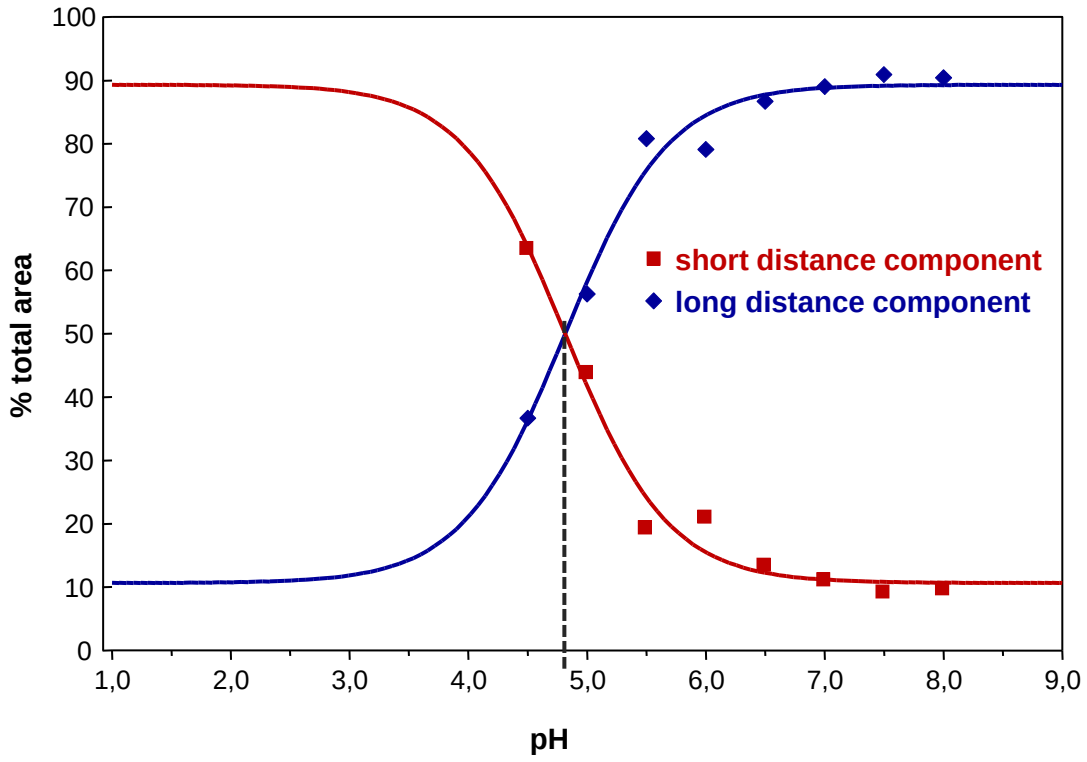

Supplementary Figure 7 | LmrP displays an apparent pKa of 4.8 for the pH-induced conformational switch. A logarithmic fit of the areas for short and long distance component peaks (red and blue curves, respectively) was performed using Prism software, showing a titration-like pH dependence.

Supplementary Figures

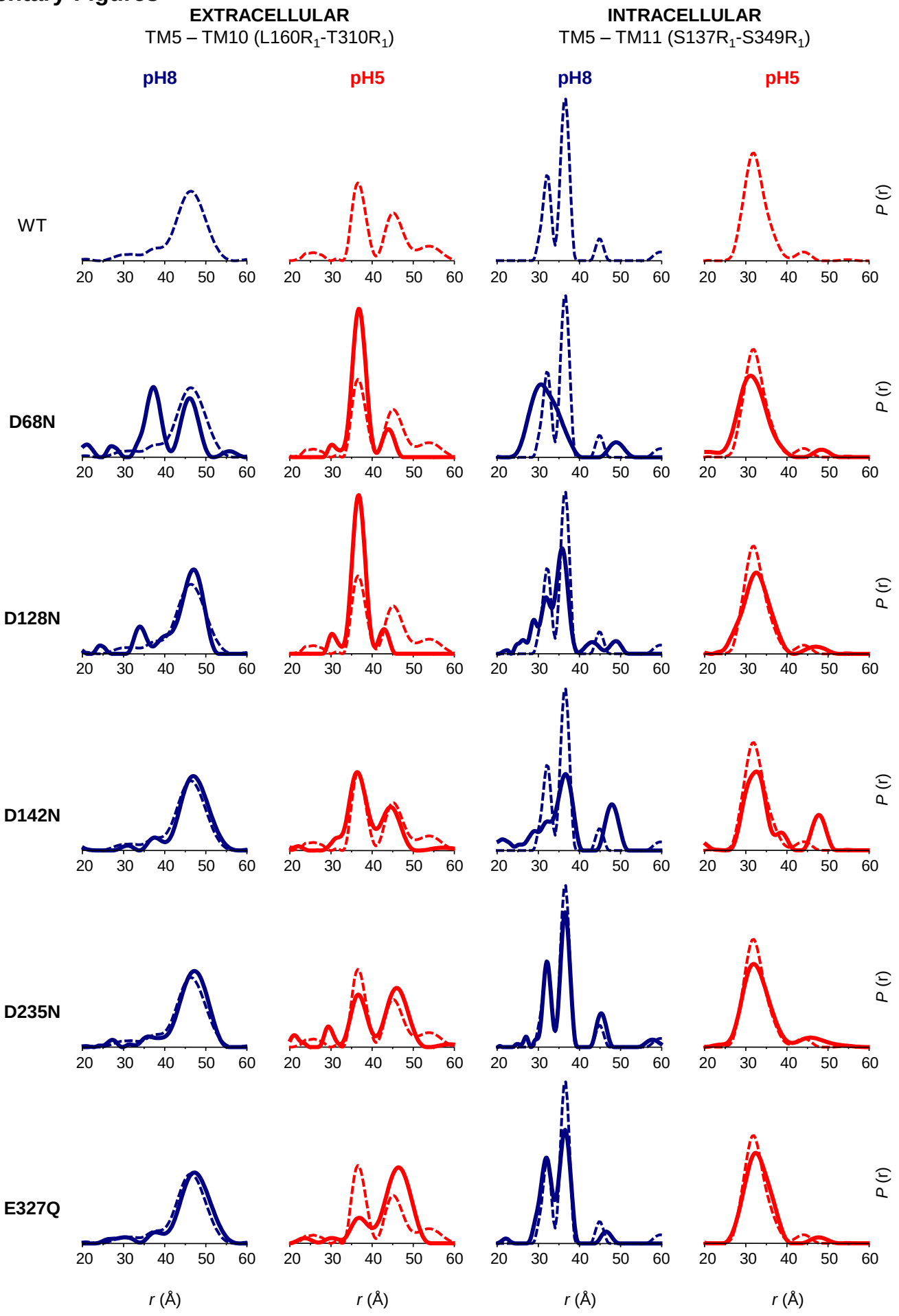

Supplementary Figure 8 | Protonation of key acidic residues can block the conformational switch. Single mutations D68N, D128N, D142N, D235N or E327Q were individually combined with double cysteine mutants L160C–I310C or V137C–S349C, which served as extracellular and intracellular reporters. Distance measurements at pH 5 (red curves) and pH 8 (blue curves) in the absence (dashed line) and presence (full line) of each mutation reveal the structural consequence of permanent protonation of these essential acidic residues.

Supplementary Figures

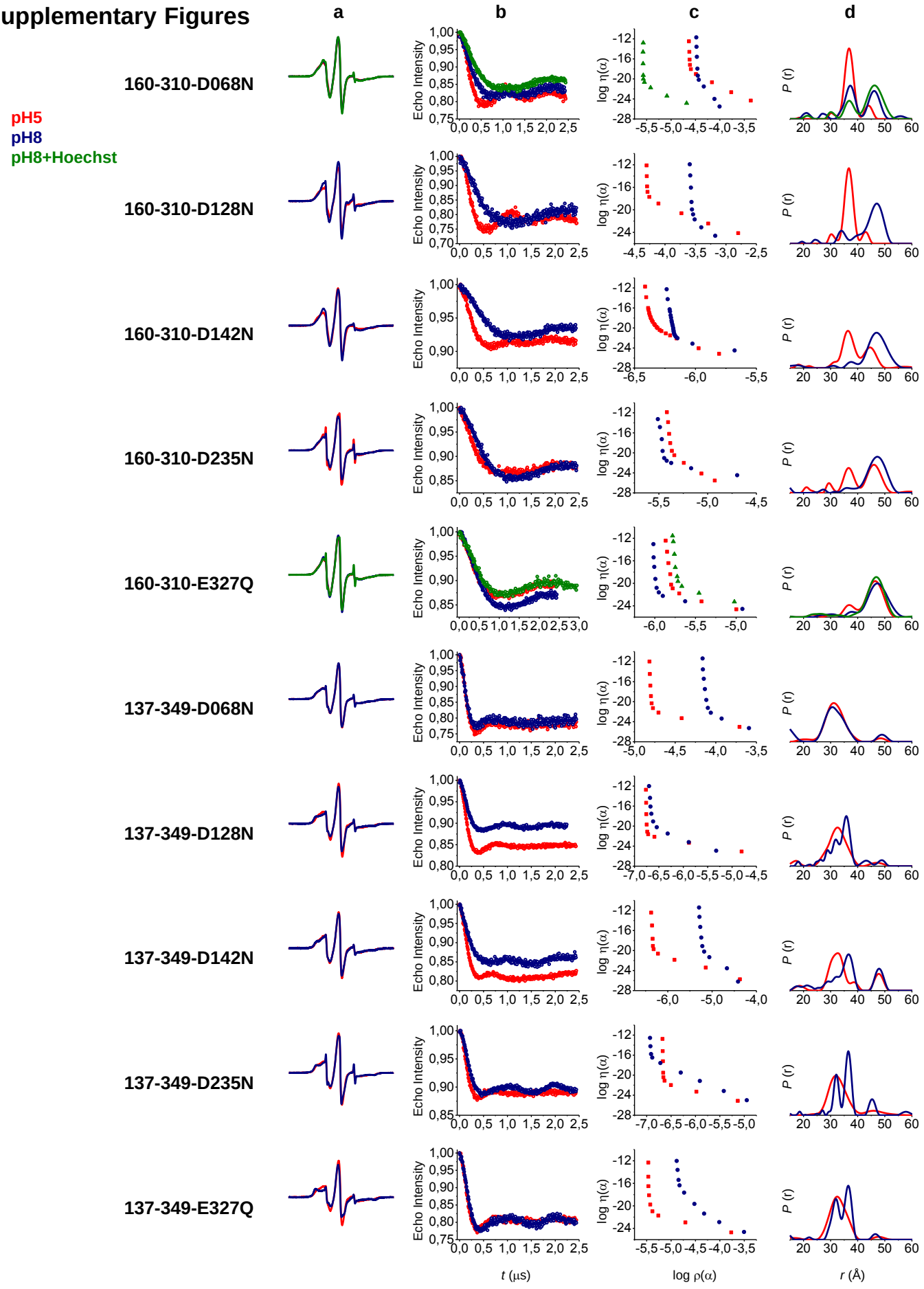

Supplementary Figure 9 | CW-EPR and DEER signal analysis of intracellular and extracellular reporter pairs V137C–S349C and L160C–I310C in the WT or mutant backgrounds (D68N, D128N, D142N, D235N, E327Q). (**a**) EPR lineshapes of spin labeled pairs in DDM micelles at pH 5 (red), pH 8 (blue) and pH 8 + Hoechst 33342 (green) demonstrated little change in spin label dynamics for each intermediate state, indicating that the local environment of the spin labels does not change substantially. (**b**) Time-dependent decay of the DEER signal (circles) and the fits (line) determined from Tikhonov regularization. (**c**) The optimum regularization parameter was chosen from the elbow of the L-curves to obtain the distance distributions as shown in **Figure 3**, **Supplementary Fig.7** and panel **d**. (**d**) DEER distance distributions.

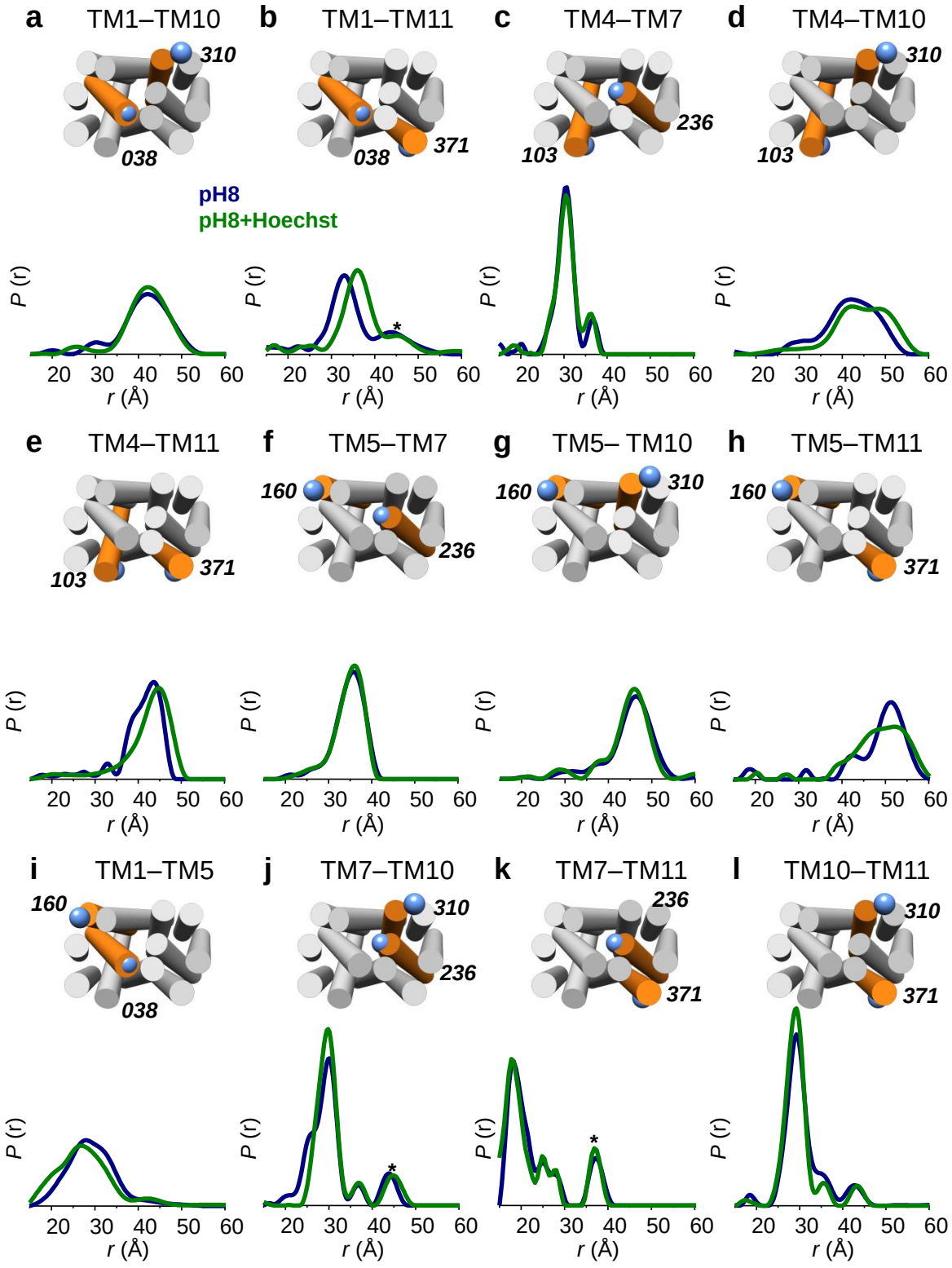

Supplementary Figure 10 | DEER distance measurements on the extracellular side in the presence (green curves) and absence (blue curves) of the LmrP substrate Hoechst 33342. The same constructs presented in **Fig. 1** were used to assess the effect of substrate binding on LmrP conformation. Residue numbers and positions of cysteine pairs are depicted on an LmrP model based on the crystal structure of the *E. coli* homolog EmrD viewed from the extracellular side. Asterisks denote peaks arising from protein aggregation.

Supplementary Figures

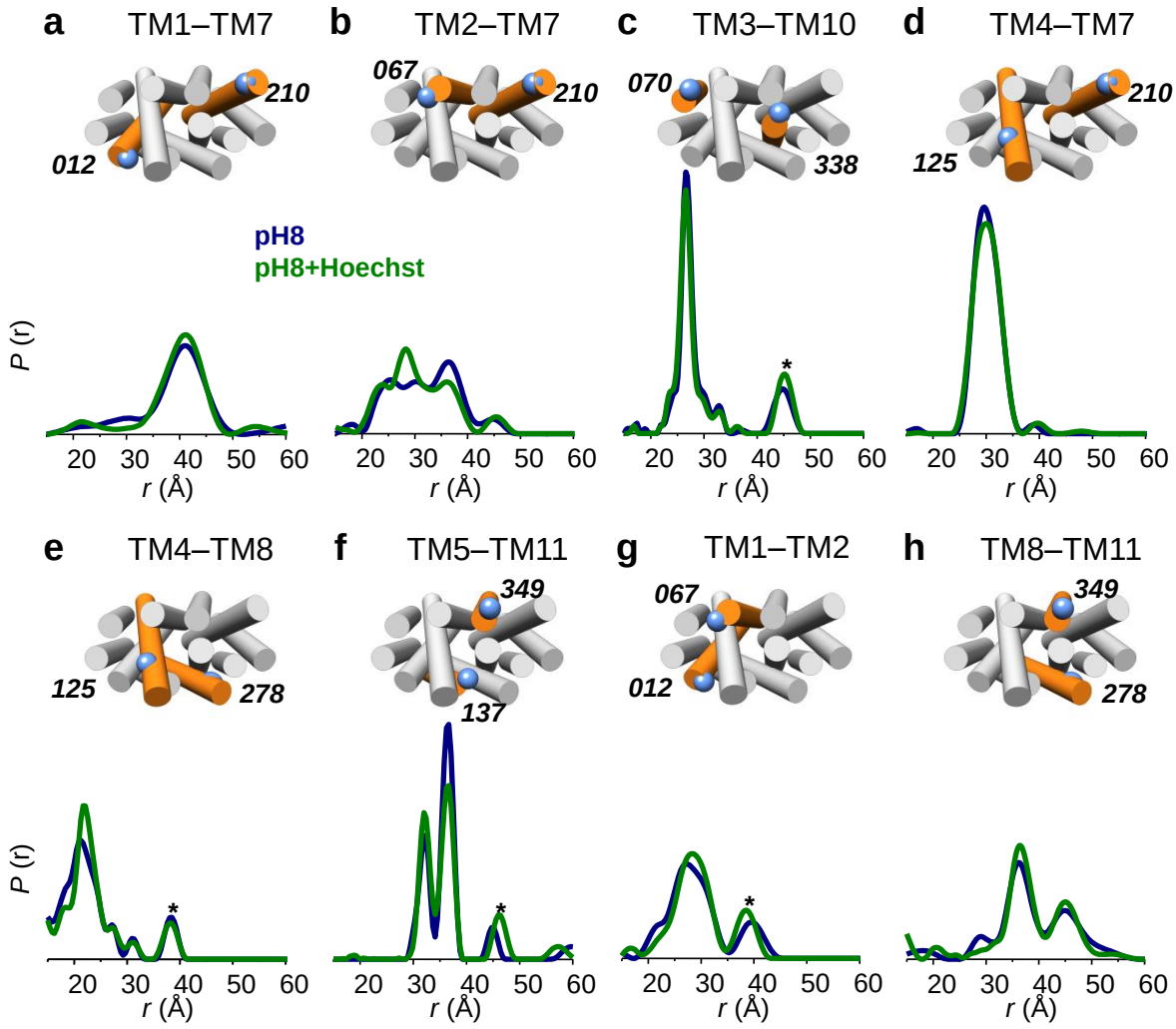

Supplementary Figure 11 | DEER distance measurements on the intracellular side in the presence (green curves) and absence (blue curves) of the LmrP substrate Hoechst 33342. The same constructs presented in **Fig. 2** were used to assess the effect of substrate binding on LmrP conformation. Residue numbers and positions are depicted on an LmrP model based on the crystal structure of the *E. coli* homolog EmrD viewed from the intracellular side. Asterisks denote artifactual peaks.

Supplementary Figures

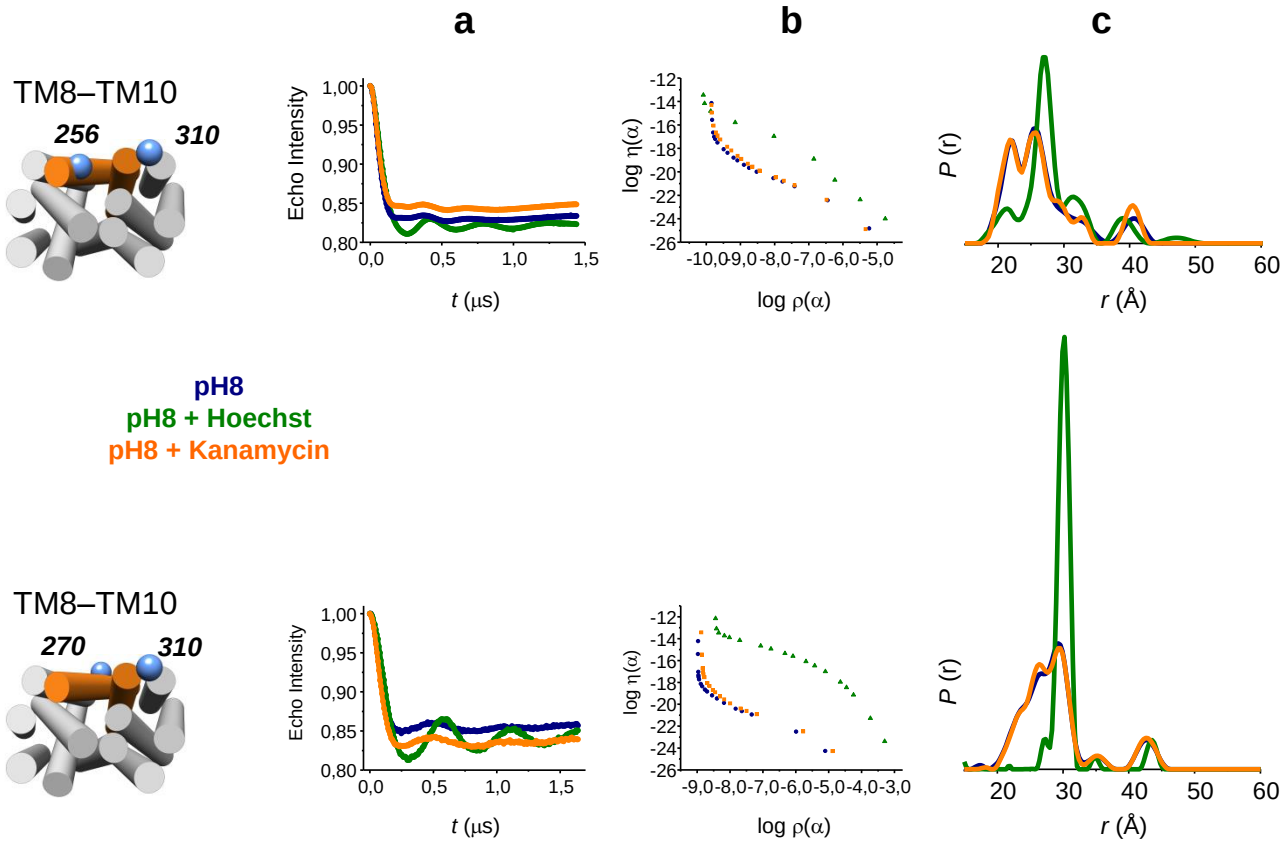

Supplementary Figure 12 | Conformational changes involving TM 8 are Hoechst 33342 - specific. Addition of 1 mM Kanamycin (orange curves), a molecule not transported by LmrP, does not induce the changes in the distance distributions for 256 – 310 and 270 – 310 as observed in the presence of 1 mM Hoechst 33342 (green curves). Residue numbers and positions of cysteine pairs are depicted on an LmrP model based on the crystal structure of the *E. coli* homolog EmrD viewed from the extracellular side. (**a**) Time-dependent decay of the DEER signal (circles) and the fits (line) determined from Tikhonov regularization. (**b**) The optimum regularization parameter was chosen from the elbow of the L-curves to obtain the distance distributions shown in panel **c**.

Supplementary Figures

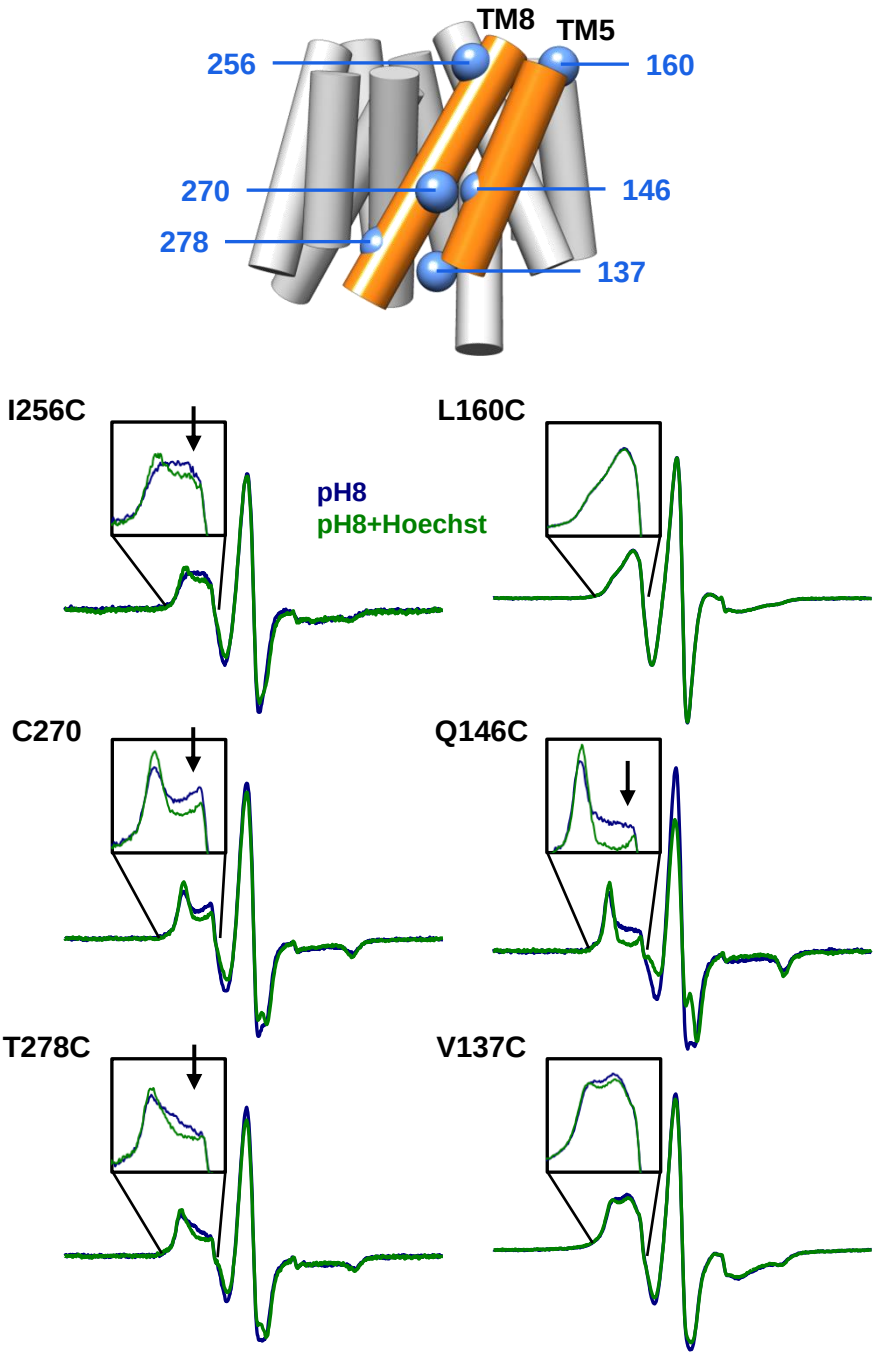

Supplementary Figure 13 | Substrate binding restricts flexibility of the outward-open conformation. A considerable substrate effect is observed on TM8 by continuous-wave EPR measurements on spin-labeled single cysteine mutants. Substrate addition decreases probe mobility for I256C, Cys270 and T278C, with the strongest effect on Cys270, located in the middle of helix 8, close to the substrate binding pocket. For equivalent residues on TM5, only Q146C, facing the predicted binding pocket cavity, is affected by substrate binding. Black arrows indicate the largest decrease in probe mobility between pH 8 (blue spectra) and pH 8 with 1 mM Hoechst 33342 (green spectra). Residue numbers and positions are depicted on an LmrP model, viewed from the side, parallel to the membrane plane, based on the crystal structure of the *E. coli* homolog EmrD.